Building Simulation 2009

*Eleventh International IBPSA Conference*
**Glasgow, Scotland**
**July 27-30, 2009**

# DEVELOPMENT OF AN AIR-BASED OPEN LOOP BUILDING-INTEGRATED PHOTOVOLTAIC/THERMAL SYSTEM MODEL

Luis Candanedo, William O'Brien and Andreas Athienitis
Solar and Lighting Laboratory
Department of Building Civil and Environmental Engineering, Concordia University
Montreal, Quebec, Canada
luismiguel_78@hotmail.com, w_obrie@encs.concordia.ca, aathieni@encs.concordia.ca

## ABSTRACT

This paper develops convective heat transfer coefficients for several different BIPV/T system configurations using Computational Fluid Dynamics models. The results for one of the CFD cases are validated with experimental data from a BIPV/T installation. The second part of the paper describes a model which is used to generate annual performance data for the system, including thermal and electrical energy production. Framing elements increase the turbulence which in turns increases the convective heat transfer coefficients. The optimal airspeed in the channel is a function of its length, weather conditions and the final required exit air temperature.

## INTRODUCTION

Building-Integrated Photovoltaic/Thermal (BIPV/T) systems produce electrical and thermal energy thus having the potential to collect more energy per unit area than individual building-integrated PV systems and solar air collectors. In open loop air-based BIPV/T systems, the heated air can be used for different purposes such as space heating, domestic hot water heating and clothes drying. BIPV/T systems consist of three layers. The outer layer consists of PV modules, the middle layer is an air channel, and the back layer is an insulated surface. By using PV modules on the outer layer, the need for traditional roofing materials such as asphalt shingles is eliminated. The framing that supports the PV modules also serves to increase turbulence in the air channel, which promotes heat transfer to the air. The waste heat from the PV modules is transferred to the airstream. Another benefit is that the PV modules are cooled, which leads to improved performance.

Bazilian and Prasad (2002), Eicker (2003), Charron and Athienitis (2006) have shown that most existing models assume the following: a) convective heat transfer correlations developed for ducts or pipes which inherently assume constant heat flux across the boundaries, constant temperature, heating symmetry and constant cross sections, b) the effect of moisture content in the air and turbulence caused by framing are ignored.

Previous work by Chen et al. (2007) and Candanedo et al. (2007) both used the upwind scheme with control volumes where the energy balance equations are solved. Computational Fluid Dynamics (CFD) simulations for a BIPV/T façade configuration has been performed with the use of a constant reference temperature for determination of the convective heat transfer coefficients (Liao et al., 2007). Determination of convective heat transfer coefficients (CHTC) for a BIPV/T façade has also been performed using Fluent (Bloem, 2004; Bloem, 2008), however the values of such coefficients were not reported. He determined the CHTCs for specific designs based on CFD simulations. Finally, the thermal network model described in detail allows whole-year simulations to be performed in order to properly characterize the collector.

## CFD SIMULATION

The commercially available CFD program, FLUENT (2006), was used as a tool to reproduce the fluid and heat transfer phenomena for a BIPV/T configuration. By postprocessing the thermal and fluid dynamics data, the CHTCs for different geometries were computed.

Figure 1 shows the PV modules and the framing used for mounting the modules in the Northern Light Canadian Solar Decathlon House.

Experimental thermal data indicate that heat transfer in such BIPV/T applications does not vary significantly along the width of the channel Candanedo et al. (2008). Therefore, it is concluded that a 2D CFD model can represent the behaviour of the system.

*Figure 1. Photo of the BIPV-T installation found at the Northern Light Canadian Solar Decathlon 2005 house.*

### Geometry and Meshing

The geometry under study consisted of a 2.84 m long by 0.04 m high air gap between the top plate (PV) and the bottom representing the roofing material. The simulation also included coupling with a solid zone attached to the back representing insulation which

allowed the model to be tested for different insulation levels. The model employed an enhanced wall treatment for the nodes close to the wall boundaries in order to improve the numerical results. In order to ensure appropriate wall treatment is necessary to check the $y^+$ values of the walls.

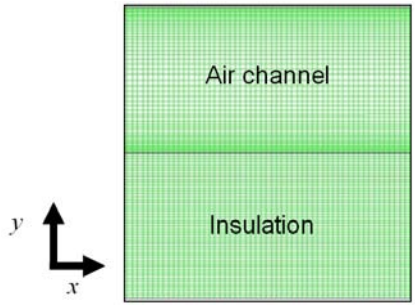


*Figure 2. Portion of the mesh employed for the CFD simulation. The top represents the fluid zone and the bottom the insulation.*

The wall $y^+$ is a non-dimensional parameter defined by the equation (Fluent, 2006)

$$y^+ = \frac{\rho u_t y_p}{\mu} \quad (1)$$

where $y_P$ is the distance from point $P$ to the wall and $\rho$ is the density of the fluid, where $u_t$ is the friction velocity, given by the equation, (Fluent, 2006) and $\mu$ is the fluid viscosity at the point P.

$$u_\tau = \sqrt{\frac{\tau_w}{\rho}} \quad (2)$$

where $\tau_\omega$ is the wall-shear stress.

As seen in equations 1 and 2, the $y^+$ value depends on the fluid viscosity and the shear stresses. The $y^+$ values depend on the velocities present in the fluid domain.

The mesh consisted of 2000 divisions along the $x$ direction and 50 divisions along the $y$ direction. For the use of enhanced wall treatment, it is recommended to have $y^+$ values in the order of 1 to 5 (Fluent, 2006). For the velocity range considered (0.5 to 1.6 m/s) the range of the $y^+$ values ranged between 0.4 to 3, which confirms that the mesh employed is adequate for the CFD code.

**Radiation modelling**

The discrete transfer radiation model (DTRM) was employed for the simulations. The model assumes that all the surfaces are diffuse and gray. The fluid is modeled as non participating media for the radiation exchange.

**Buoyancy**

The fluid density is treated using the incompressible ideal gas law,

$$\rho = \frac{p_{op}}{\frac{R}{M_w}T} \quad (3)$$

where $R$ is the universal gas constant, $M_w$ is the molecular weight of the gas and $p_{op}$ is the operating pressure.

The thermal conductivity ($k$) of the fluid was assumed to be a weighed average of dry air with moist air. Gravity is considered in the model as well.

**Turbulence model**

The standard $\kappa$-$\omega$ model was used for the simulations. This was done after a series of comparisions between turbulence models for a similar geometry showed the $\kappa$-$\omega$ turbulence model gave the most accurate results (Candanedo et al., 2008).

**Definition of the CHTC**

The CHTC is defined by:

$$h_c = abs\left(\frac{q_c}{(T_{wall} - T_{bulk})}\right) \quad (4)$$

where $q_c$ is the convective heat flux (defined as the total surface heat flux minus the radiative heat flux), $T_{wall}$ is the surface temperature and $T_{bulk}$ is a representative temperature (sometimes also called mixed-cup temperature) for the cross section of the channel (Incropera and De Witt, 2002). $h_c$ is required to be always positive in order to be used in thermal network modeling and avoid nonsensical results.

The asymmetric heating condition causes large temperature gradients across the fluid domain. The local bulk temperature was found by integration. Since it is not done automatically by FLUENT, the local bulk air temperature had to be calculated using the following definition (Oosthuizen and Naylor, 1999):

$$T_{bulk} = \frac{\int_A \rho u T dA}{\int_A \rho u dA} \quad (5)$$

where $\rho$ is the fluid density, $u$ is the velocity in the stream direction, $T$ is the fluid temperature and $dA$ is the face volume area.

**Boundary conditions**

The boundaries conditions and their types are summarized in Figure 3 and explained in Table 1.

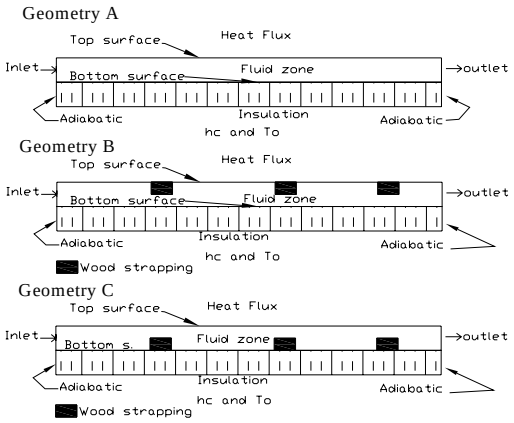


*Figure 3. Schematics of the three different geometries tested with CFD analysis.*

**Table 1: Summary of boundaries and their types**

| | Type | | |
|---|---|---|---|
| **Boundary** | Momentum | Thermal | Species |
| **Top s.** | No slip | Constant Heat Flux | No |
| **Bottom s.** | No slip | Coupled | No |
| **Inlet** | Velocity inlet | T = 300K | Constant |
| **Outlet** | Pressure outlet | | Constant |
| **Insulation** | N.A. | Coupled | No |
| **Wood Strap.** | No slip | Coupled | No |
| **Bottom Insulation** | N.A. | Convective h & T | No |

For the interior surfaces the walls were asumed to be smooth except for the ones where wood strapping was present and a rugosity value was employed.

## CASES STUDIED

1-Straight channel, low heating (q = 200 W/m$^2$), different speeds. 1.5 RSI. Geometry A.

2-Smooth channel, different level of insulation, same speed (V = 0.50 m/s) Geometry A.

3-Straight channel, strapping on the bottom. (q = 200 W/m$^2$) 1.5 RSI. Geometry C.

4-Straight channel, strapping on the top. (q = 200 W/m$^2$) 1.5 RSI. Geometry B.

5-Straight channel, higher heat flux (q = 400 W/m$^2$) 1.5 RSI. Geometry A.

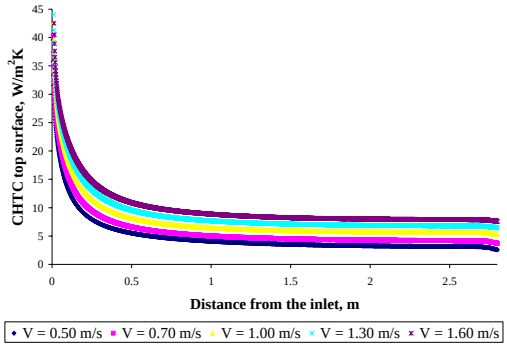


*Figure 4. CHTCs for the top surface smooth channel for different air speeds (Case 1).*

Figure 4 shows the CHTC for Case 1. The average values are 4.85, 5.98, 7.57, 8.87 and 10.11 W/m$^2$K for the velocities of 0.50, 0.70, 1.00, 1.30 and 1.60 m/s, respectively.

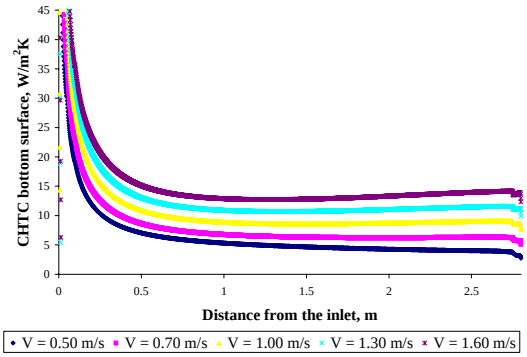


*Figure 5. CHTC bottom surface channel for different airspeeds (Case 1).*

Figure 5 shows that the CHTC starts to increase slightly towards the exit of the channel for speeds above 1.30 m/s. The average CHTC values are 6.7, 8.37, 10.94, 13.36 and 15.67 W/m$^2$K for the velocities of 0.50, 0.70, 1.00, 1.30 and 1.60 m/s, respectively.

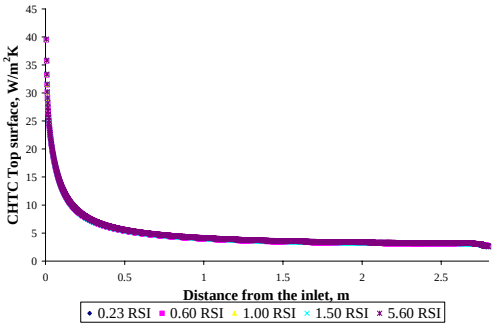


*Figure 6. CHTC for the top surface with insulation variation for an air speed of 0.5 m/s (Case 2).*

Figure 6. shows that the CHTC for the top surface experiences almost no variation by increasing the insulation level.

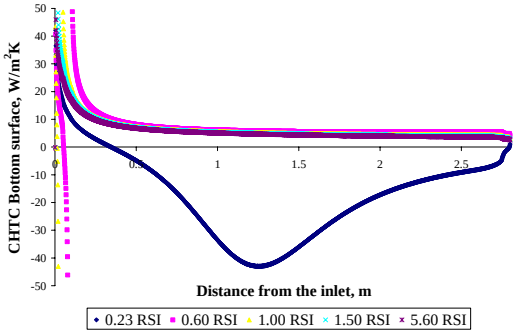


*Figure 7. CHTC for the bottom cavity surface for different insulation levels (Case 2).*

The negative sign in Figure 7 is shown to indicate in the same image the direction of the heat flux. When the CHTC is negative, the bulk air temperature is higher than the temperature of the wall surface. This means that for the case of very low insulation (0.230 RSI) the heat loss from the bottom surface to the exterior is significant causing the surface temperature of the interior side of the insulation to be lower than the bulk air temperature.

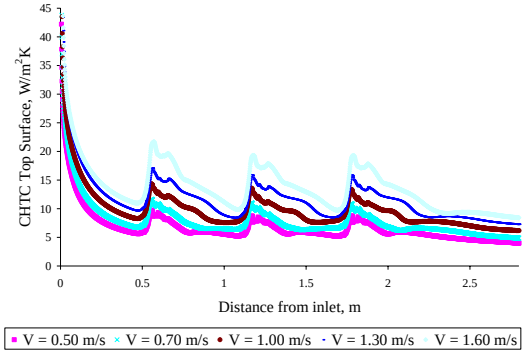


*Figure 8. CHTCs for the top surface for different airspeeds for strapping on the bottom (Case 3).*

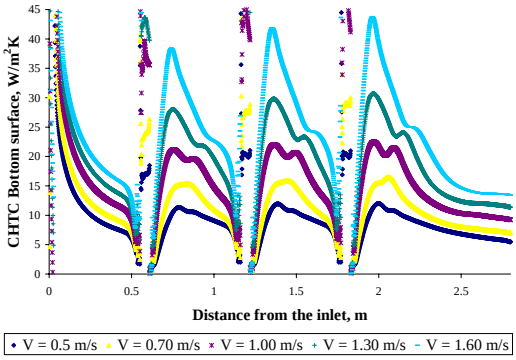


*Figure 9. CHTC for the bottom surface for different airspeeds for strapping on the bottom (Case 3).*

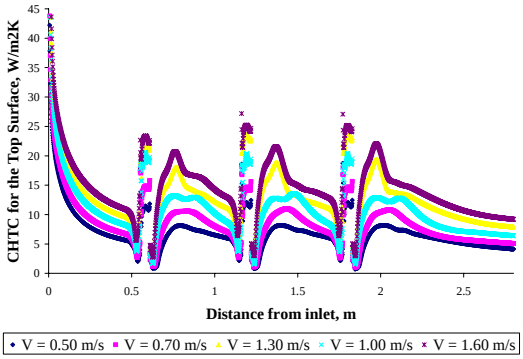


*Figure 10. CHTCs for the top surface for different airspeeds for the top strapping case (Case 4).*

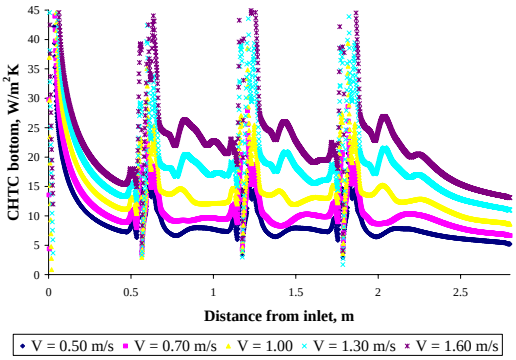


*Figure 11. CHTCs for the bottom surface for different airspeeds for the top strapping case (Case 4).*

Figures 10 and 11 show the local CHTCs for the top and bottom surfaces. The peaks occur where the wood strapping is present.

Cases 3 and 4 demonstrate that the strapping on the top surface has higher average CHTC values than the ones on the bottom.

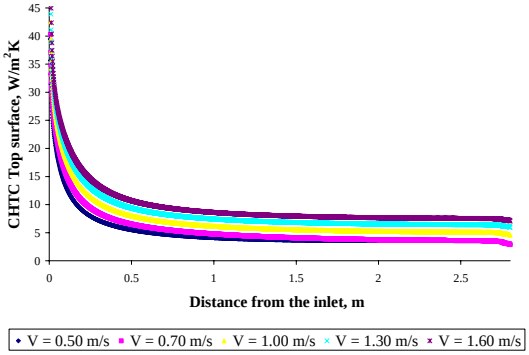


*Figure 12. CHTCs for the top cavity surface for different airspeeds and a higher heat flux (q= 400 W/m$^2$) (Case 5).*

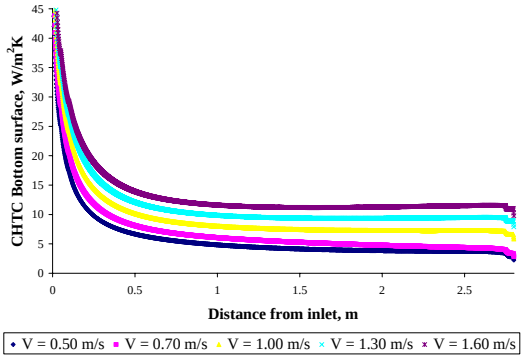


*Figure 13. CHTCs for the bottom surface for different air speed and higher heat flux (q= 400 W/m$^2$) (Case 5.)*

Figures 12 and 13 show that there is no significant difference in the shape of the curves for Case 1 when the heat flux was halved. However, the averaged

bottom coefficients were 12% lower than the case with higher heat flux. They were also lower by around 3% for the top surface.

## EXPERIMENTAL VALIDATION

The experimental setup was designed with the intention of measuring CHTCs for different BIPV/T configurations. The variables measured include the incident solar radiation, mass flow rate, electrical energy production, ambient air temperature, relative humidity, wind speed, surface and air temperature profiles along the stream direction, surface optical properties, and inlet and outlet average temperatures.

*Figure 14. Left: experimental BIPV/T setup right: solar air collector.*

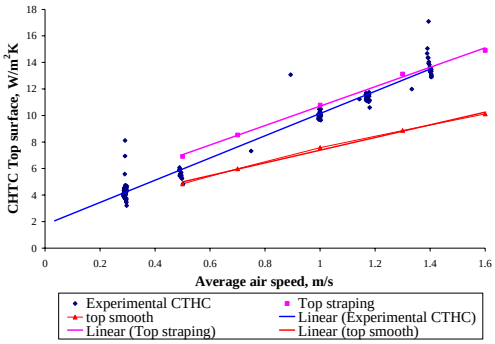


*Figure 15. Left: experimental BIPV/T setup and right: solar air collector.*

Experimental average CHTCs for the top surface are shown in Figure 15. These are compared with the CHTCs for the top surface for Cases 1 and 4. The BIPV/T installation used small metal strips on the top surface to avoid inward bending. This is why the results agree more with the top strapping case. The closeness of the simulated versus the experimental (measured) CHTCs confirms the validity of the CFD results.

## BIPV/T LUMPED PARAMETER MODEL

An lumped parameter model was created to assess the energy implications of various design decisions. The model uses the upwind discretization scheme with five control volumes. This allows different CHTCs to be applied for different locations along the channel (in the direction of flow). This is particularly important for our purposes because we are interested in studying the effects of different local CHTCs. The model is 2D and is shown in Figure 1. Two assumptions greatly increase the simplicity of the model. First, the radiative heat transfer is linearized. Second, conduction and radiation are assumed to be confined to each control volume. This is justified for two reasons: 1) the heat carried by the airflow in the channel dominates heat transfer, 2) for radiative heat transfer, the view factors for opposite surfaces is very large compared to that of the surfaces in adjacent control volumes. The nodal equations for the thermal network are provided below. The sign convention used was to assume all heat fluxes are entering the node of interest.

$$\text{PV: } G\left(\alpha - \frac{A_{PV}}{A_{roof}}\eta\right) + U_{c,o}(T_o - T_{PV}) + U_{r,o}(T_{sky} - T_{PV}) + U_{c,PV}\left(T_{air}^{i} - T_{PV}\right) + U_r(T_b - T_{PV}) = 0 \quad (6)$$

$$\text{Air: } F\left(T_{air}^{i-1} - T_{air}^{i}\right) + U_{c,PV}\left(T_{PV} - T_{air}^{i}\right) + U_{c,b}\left(T_b - T_{air}^{i}\right) = 0 \quad (7)$$

$$\text{Back: } U_a(T_a - T_b) + U_{c,b}\left(T_{air}^{i} - T_b\right) + U_r(T_{PV} - T_b) = 0 \quad (8)$$

Where

| | |
|---|---|
| $G$ | Incident solar radiation on surface |
| $\alpha$ | Area-weighted absorptivity |
| $\frac{A_{PV}}{A_{roof}}$ | Fraction of roof covered by PV modules |
| $\eta$ | Local PV cell efficiency |
| $U_{c,o}, U_a$ | Total heat transfer between the PV and outside and between the back and attic, respectively |
| $U_{c,PV}, U_{c,b}$ | Convective heat transfer to between the PV and air and between the back and air, respectively |
| $U_r, U_{r,o}$ | Radiative heat transfer between PV and back, and PV and surroundings, respectively |
| $T_{PV}, T_b$ | Temperature of PV and back, respectively |
| $T_o, T_a$ | Temperature of outdoor air and attic or roof space, respectively |
| $F$ | Specific power associated with the airflow; units: W/K |
| $T_{air}^{i}, T_{air}^{i-1}$ | Temperature of air node in current and upstream control volume, respectively |

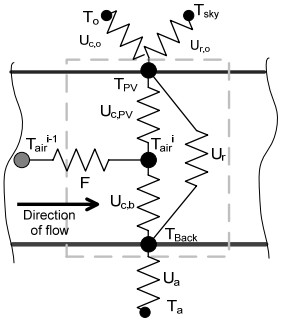


*Figure 16. A network diagram showing a single control volume of the BIPV/T model.*

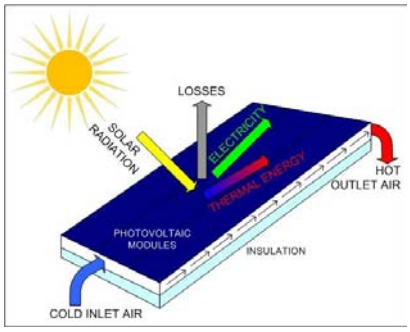


*Figure 17. Cross section of BIPV/T roof.*

Since PV modules are unlikely to cover the entire roof area, the fraction of module coverage must be considered in the model. The parts of the roof without modules transfer slightly more energy to the air because electricity is not being "tapped off". The model assumes that the modules are well-distributed on the roof.

As PV modules increase in efficiency, the importance of considering the temperature coefficient becomes more important. Not only are we interested in the electrical energy production but also the corresponding change in the portion of the incident solar energy that is transferred to the airstream. Thus, the following equation must be subbed into equation 8.

$$\eta = \eta_o\text{-}\beta T_{PV} \tag{9}$$

where,

$\eta_o$ Nominal PV module efficiency

$\beta$ Temperature coefficient of PV module

For low-efficiency PV cells, this effect has a negligible effect on thermal performance.

While there is a substantial temperature gradient of the PV cells along the direction of flow, if the cells are assumed to be wired in series, then they will operate at the local roof temperature.

For computational efficiency, the equations were converted to matrix form, as shown below. Starting from the first control volume, the three nodal temperatures are solved simultaneously using this system of equations. For the first control volume, the incoming air temperature is assumed to be the same as the outdoor air temperature. For each subsequent control volume, the incoming air is the temperature that was solved from the previous control volume. In this way, the set of equations is solved a total of five times for each time step.

$$\begin{bmatrix} -\frac{A_{PV}}{A_{roof}}\beta + U_{c,o} + U_{r,o} + U_{c,PV} + U_r & -U_{c,PV} & -U_r \\ -U_{c,PV} & F + U_{c,PV} + U_{c,b} & -U_{c,b} \\ -U_r & -U_{c,b} & U_a + U_{c,b} + U_r \end{bmatrix} \times \begin{pmatrix} T_{PV} \\ T_{air}^i \\ T_b \end{pmatrix} = \begin{pmatrix} G(\alpha - \frac{A_{PV}}{A_{roof}}\eta_o) + U_{c,o}T_o + U_{r,o}T_{sky} \\ FT_{air}^{i-1} \\ U_aT_a \end{pmatrix} \tag{10}$$

The interior CHTCs were determined from the CFD simulations. Since the CFD model mesh size was much smaller than the control volumes used for the energy performance model, the mean value for CHTCs was determined for each control volume.

## QUANTIFYING BIPV/T PERFORMANCE

The performance of BIPV/T systems is largely dependent on the application and demand profile. For instance, the minimum air temperature usefulness threshold may vary from 0 to 20°C or more. For comparative purposes, this study uses 10°C as a reference point. This is selected as the point where extracting heat from the ground using a ground source heat pump, may become more efficient. Thus, if the outlet temperature is greater than both the inlet temperature and 10°C, annual thermal energy output is determined using the following equation.

$$E_{thermal} = \sum_{hour=1}^{8760} F(T_{out} - T_{in}) \tag{11}$$

BIPV/T electrical performance is determined by summing the electrical output of each control volume and daytime hour of the year.

## RESULTS

To illustrate the performance of a BIPV/T roof as well as compare performance for several different designs, the model was used for whole year simulations. The collector modeled is 2.84 meters long (direction of flow) by 1 meter wide. It is inclined on a 45 degree slope, south-facing, and in Montreal. The PV modules have a nominal efficiency of 6.29% and a temperature coefficient of -0.11%/K. PV modules cover 80% of the roof area. For each of the following four cases, the outlet temperature profile is shown on a design day, along with annual performance.

### Nominal Case (Case 1)

This is the base case, with smooth interior surfaces and insulation on the back surface equivalent to RSI-1.5. Five flow rates were examined. The results show that increasing the airspeed has a positive effect on thermal energy output, but at the cost of having lower outlet air temperatures. This suggests that airspeed should be controlled to maximize energy output while ensuring that the outlet temperature is suitable for the intended application. The effect on electrical performance is negligible.

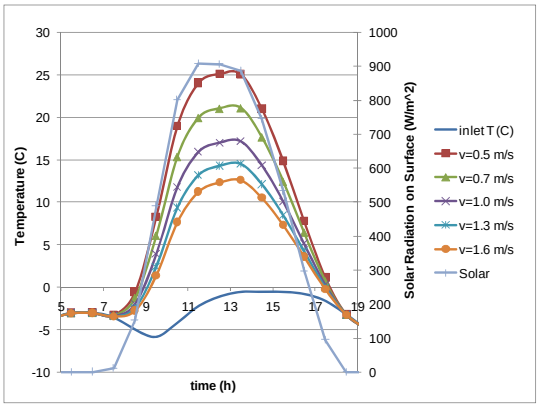


*Figure 18. Design day outlet air temperature profiles for the nominal case.*

**Table 2: Performance for the nominal case**

| | Channel Airspeed (m/s) | | | | |
|---|---|---|---|---|---|
| | **0.5** | **0.7** | **1.0** | **1.3** | **1.6** |
| **DD Thermal (kWh)** | 3.928 | 4.649 | 5.448 | 5.912 | 6.360 |
| **DD Electricity (kWh)** | 0.808 | 0.811 | 0.814 | 0.816 | 0.818 |
| **Annual Thermal (kWh)** | 843.1 | 969.5 | 1106.4 | 1189.5 | 1254.7 |
| **Annual Electricity (kWh)** | 190.4 | 190.9 | 191.4 | 191.8 | 192.1 |
| **Peak Annual Temp. (C)** | 56.5 | 52.9 | 49.3 | 46.7 | 44.9 |

## Varying Insulation (Case 2)

The results of varying the level of insulation on the back surface demonstrates two things: 1) a fairly significant improvement can be achieved with the addition of insulation and 2) beyond about 1.5 $m^2K/W$, there is little opportunity for improvement in performance and the cost of the extra insulation is not likely justified.

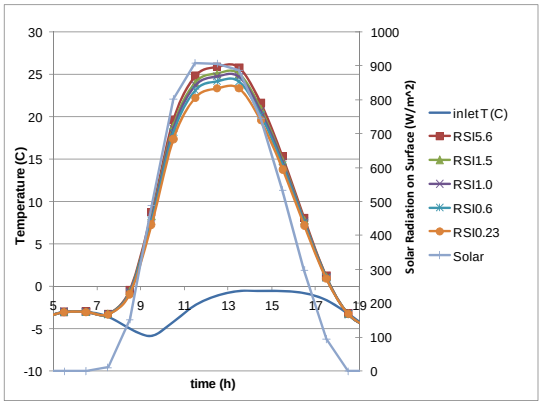


*Figure 19. Design day outlet air temperature profiles for varying insulation*

**Table 3 Performance for varying insulation**

| | Insulation level (RSI – $m^2K/W$) | | | | |
|---|---|---|---|---|---|
| | **0.2** | **0.6** | **1.0** | **1.5** | **5.6** |
| **DD Thermal (kWh)** | 3.660 | 3.790 | 3.875 | 3.928 | 4.046 |
| **DD Electricity (kWh)** | 0.810 | 0.809 | 0.809 | 0.808 | 0.808 |
| **Annual Thermal (kWh)** | 779.4 | 809.1 | 830.3 | 843.1 | 872.2 |
| **Annual Electricity (kWh)** | 190.7 | 190.5 | 190.4 | 190.4 | 190.3 |
| **Peak Annual Temp. (C)** | 55.1 | 55.7 | 56.2 | 56.5 | 57.2 |

## Bottom Strapping (Case 3)

The addition of wood strapping on the bottom surface, results in an additional thermal energy output of about 15%. However, the addition of strapping or other obstacles must be balanced with the increased pressure drop and corresponding increase in fan energy consumption. PV performance is only modestly superior with the addition of strapping on the bottom surface.

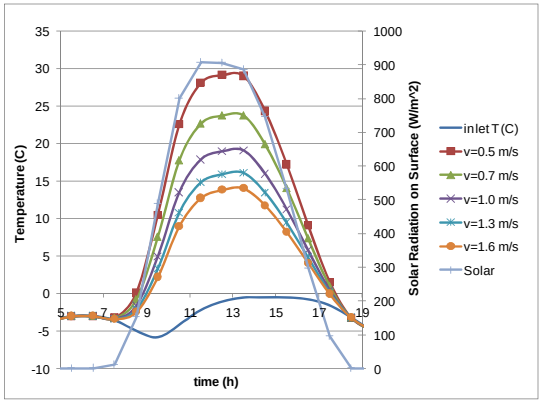


*Figure 20. Design day outlet air temperature profiles for bottom strapping*

**Table 4 Performance for bottom strapping**

| | Channel Airspeed (m/s) | | | | |
|---|---|---|---|---|---|
| | **0.5** | **0.7** | **1.0** | **1.3** | **1.6** |
| **DD Thermal (kWh)** | 4.661 | 5.224 | 6.027 | 6.634 | 7.046 |
| **DD Electricity (kWh)** | 0.811 | 0.813 | 0.817 | 0.819 | 0.821 |
| **Annual Thermal (kWh)** | 994.5 | 1114.3 | 1246.2 | 1337.9 | 1413.6 |
| **Annual Electricity (kWh)** | 190.8 | 191.3 | 191.8 | 192.2 | 192.6 |
| **Peak Annual Temp. (C)** | 60.4 | 55.6 | 51.2 | 48.3 | 46.3 |

**Top Strapping (Case 4)**

For the case with strapping on the top surface (i.e., directly below the PV modules), performance is slightly better than the case with strapping on the bottom. This is because heat transfer from the top surface – where the heat is being generated – is enhanced. However, the strapping for both surfaces is necessary to support the PV module. This case is still remaining to be simulated.

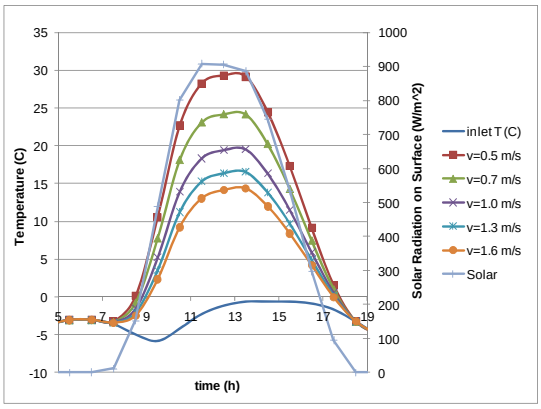


*Figure 21. Design day outlet air temperature profiles for top strapping*

**Table 5: Performance for top strapping**

| | Channel Airspeed (m/s) | | | | |
|---|---|---|---|---|---|
| | **0.5** | **0.7** | **1.0** | **1.3** | **1.6** |
| **DD Thermal (kWh)** | 4.693 | 5.311 | 6.163 | 6.841 | 7.194 |
| **DD Electricity (kWh)** | 0.811 | 0.814 | 0.817 | 0.820 | 0.822 |
| **Annual Thermal (kWh)** | 1002.0 | 1136.7 | 1274.6 | 1383.1 | 1447.9 |
| **Annual Electricity (kWh)** | 190.8 | 191.3 | 191.9 | 192.4 | 192.7 |
| **Peak Annual Temp. (C)** | 60.5 | 55.9 | 51.6 | 48.8 | 46.6 |

## CONCLUSION

This paper presented a detailed numerical study and model of a BIPV/T roof with an open loop air-based heat recovery system. A CFD method was used to obtain convective heat transfer coefficients under different flow rates and design options. The simulation shows that insulation should be at least RSI-1.5.A lumped parameter model was also presented. Electrical efficiency is slightly increased with higher flow rates. This effect becomes more significant with higher efficiency PV modules. The optimum airflow rate will depend on the channel geometry and the outlet air temperature requirements. The following important parameters are under further study: pressure drop and fan energy consumption, the effect of using a higher electrical efficiency on the panels, and whole system modelling, including demand profiles and storage.

## REFERENCES


Bazilian, M.D., and D. Prasad. 2002. Modelling of a photovoltaic heat recovery system and its role in a design decision support tool for building professionals. Renewable Energy 27:57-68.

Bloem, J.J. 2004. A TRNSYS type calculation model for double skin photovoltaic facades. Proc. 19th European Photovoltaic Solar Energy Conference and Exhibition, Paris, France, 2004.

Bloem, J.J. 2008. Evaluation of a PV integrated building application in a well controlled outdoor test environment. Building and Environment. 43:205-216.

Candanedo, J.A., S. Pogharian, A.K. Athienitis, and A. Fry. 2007. Design and simulation of a net zero energy healthy home in Montreal. 2nd Canadian Solar Buildings Conference. 1:1-8.

Candanedo, L.M., C. Diarra, A. Athienitis, and S. Harrison. 2008. Numerical modelling of heat transfer in photovoltaic-thermal air-based systems. In 3nd Canadian Solar Buildings Conference. Vol. 1. S.B.R. Network, editor, Fredericton, Canada.

Charron, R., and A.K. Athienitis. 2006. A two dimensional model of a double facade with integrated photovoltaic panels. Journal of Solar Energy Engineering, ASME. 128:160-167.

Chen, Y., A.K. Athienitis, B. Berneche, Y. Poissant, and K.E. Galal. 2007. Design and simulation of a building integrated photovoltaic-thermal system and thermal storage for a solar house. Proc. 2nd Canadian Solar Buildings Conference.

Eicker, U. 2003. Solar technologies for buildings, West Sussex.First Edition.

FLUENT Inc. 2006. FLUENT 6.3 User's Guide, Lebanon

Incropera, F.P., and D.P. De Witt. 2002. Fundamentals of heat and mass transfer. John Wiley & Sons. 981 pp.Fifth

Liao, L., A.K. Athienitis, L. Candanedo, K.-W. Park, Y. Poissant, and M. Collins. 2007. Numerical and Experimental Study of heat transfer in a BIVP-Thermal system. Journal of Solar Energy Engineering, ASME. 129:423-430.

Oosthuizen, P.H., and D. Naylor. 1999. An introduction to convective heat transfer analysis. McGraw Hill. 620 pp